# A Stochastic Linear Theory of Mesoscale Circulation Induced by the Thermal Heterogeneity of the Land Surface

JINGFENG WANG, RAFAEL L. BRAS, AND ELFATIH A. B. ELTAHIR

*Department of Civil and Environmental Engineering, Massachusetts Institute of Technology, Cambridge, Massachusetts*

(Manuscript received 21 August 1995, in final form 28 May 1996)

ABSTRACT

This paper presents a three-dimensional stochastic linear model of the mesoscale circulation induced by the variability of turbulent sensible heat flux over land surface. The primitive equations relating wind field, geopotential, and potential temperature are formulated as a system of stochastic partial differential equations and solved analytically. The solution is based on spectral representations of homogeneous random fields. The flow intensity is found to be proportional to the standard deviation of the turbulent sensible heat flux into the atmosphere. Large (small) scales of spatial variability in the surface heating preferably impact circulations at high (low) altitudes. The mesoscale fluxes associated with the atmospheric flow are related to explicit functions of atmospheric stability, variance of turbulent heat flux, and synoptic wind. The authors find that the vertical momentum flux is significant in the presence of synoptic wind and that the flow perpendicular to the direction of the synoptic wind is responsible for this momentum flux. The proposed linear theory identifies the synoptic conditions under which the land-surface heterogeneity may play a role in atmospheric circulations at the mesoscale.

## 1. Introduction

Natural variability in vegetation cover and soil types over large areas induces variability in turbulent heat fluxes into the atmosphere. These nonuniform heat fluxes often exhibit irregular patterns with length scales ranging from meters to hundreds of kilometers. In some cases, surface temperature differences of about 10°C are observed over distances of 10–20 km (Segal et al. 1988), and more than 200 W $m^{-2}$ differences in sensible heat flux are observed over similar distances (Sun and Mahrt 1994). Satellite observations demonstrate that these thermal heterogeneities are also evident over larger scales (e.g., Segal et al. 1988; Pielke et al. 1991). Such heterogeneity of the land surface is expected to induce mesoscale circulations analogous to a sea breeze. Rabin et al. (1990) suggest that under some synoptic conditions land-surface heterogeneities may have a significant impact on the mesoscale circulations.

In recent years, there has been increasing interest in the characterization of the impact of variability of land surface on the dynamics of the mesoscale circulation and the associated energy and mass transport in large-scale atmospheric models. Theoretical approaches (e.g., Rotunno 1983; Dalu and Piekle 1989; Dalu et al. 1991) and numerical simulations (e.g., Avissar and Pielke 1989; Avissar and Chen 1993; Lynn et al. 1995a,b) have argued that the intensity of the mesoscale circulation induced by the thermal heterogeneity of land surface could be as strong as the sea breeze and that the associated mesoscale heat flux can be as large as the turbulent heat flux.

Rotunno (1983) developed a two-dimensional linear land- and sea-breeze model to investigate the atmospheric response to the periodic diurnal cycle of heating and cooling due to the contrast between land and sea. His paper provides a good review of the theoretical studies of sea breeze up to the early 1980s. He showed that the flow is either of elliptic or of hyperbolic type depending on the latitude. The 30° latitude is identified as the boundary dividing the two regimes. Dalu and Pielke (1989, 1993) and Dalu et al. (1991) extended Rotunno's work to study the effects of the nonperiodic forcing and the effects of friction. For a realistic magnitude of friction, they found that only an elliptic solution is possible. The vertical heat flux generated by the landscape-induced mesoscale circulation has been shown to be of the same order as the diabatic sensible heat flux. The previous analytical studies do not deal with the issue of water balance of the atmosphere.

In this paper a stochastic linear theory is developed to investigate the conditions under which the thermally induced mesoscale circulations and the associated mesoscale fluxes are important. A 3D linearized dynamic system, including the effects of a constant synoptic wind, is formulated to model the mesoscale cir-

*Corresponding author address:* Dr. Jingfeng Wang, Dept. of Civil and Environmental Engineering, Massachusetts Institute of Technology, 48-320, Ralph M. Parsons Laboratory, Cambridge, MA 02139-4307.

culation driven by the diabatic heating due to the turbulent sensible heat flux. The variable sensible heat flux over the land surface is described by a 2D homogeneous random field. Wind velocity components, pressure, temperature, and moisture content vary randomly in response to the random surface heating. Hence they can be expressed using spectral representations of homogeneous random fields. The temporal and vertical distributions of these state variables are related to the parameters characterizing the synoptic environments through the governing equations for the atmospheric flows. The intensities of the mesoscale circulation and the mesoscale fluxes are computed using an analytical solution of the stochastic partial differential equations relating the wind velocities, pressure, temperature, and moisture content to the random diabatic forcing.

Three major improvements over the previous analytical work have been achieved in the stochastic linear theory presented in this paper. First, a three-dimensional model is adopted. All the aforementioned theoretical studies utilize two-dimensional models. Second, the thermal inhomogeneity of land surface in our 3D model is characterized by a 2D random field that realistically represents the complexity of natural landscape. This is in contrast to the oversimplified landscape patterns, in the form of periodic warm–cool stripes, that were assumed by previous studies. Third, the effects of synoptic wind are studied quantitatively. To our knowledge, this issue has not been addressed in previously published analytical work. As we will show in the following, an advantage of the 3D model is that it can predict the vertical momentum flux (resulting from the wind component perpendicular to the synoptic wind) in the presence of synoptic wind while 2D models cannot. The analytical results from our 3D stochastic linear theory can be used directly in parameterization of the subgrid energy and mass transport in the large-scale atmospheric models.

Modeling of the 3D atmospheric flow and the statistical characterization of the thermal variability of the landscape are presented in section 2. The analytical solution of the governing equations will be given in section 3. Statistics of the mesoscale circulation are then discussed in section 4. The stochastic equation of water balance of atmosphere will be derived in section 5. The properties of the mesoscale fluxes will be discussed in section 6. Summary and conclusions are made in section 7.

Notations and variables are specified in appendix A. Detailed mathematical derivations also appear in the appendixes.

## 2. Stochastic modeling of 3D atmospheric flow

### a. Governing equations

The two-dimensional linear land- and sea-breeze model of Rotunno (1983) and Dalu and Pielke (1989) is generalized to three dimensions, in the presence of synoptic wind, to describe the flow driven by the gradients of diabatic heating caused by variability of the land surface. The model equations are

$$\frac{\partial u}{\partial t} + u_0 \frac{\partial u}{\partial x} - fv = -\frac{\partial \phi}{\partial x} - \alpha u \tag{1}$$

$$\frac{\partial v}{\partial t} + u_0 \frac{\partial v}{\partial x} + fu = -\frac{\partial \phi}{\partial y} - \alpha v \tag{2}$$

$$\frac{\partial w}{\partial t} + u_0 \frac{\partial w}{\partial x} - b = -\frac{\partial \phi}{\partial z} - \alpha w \tag{3}$$

$$\frac{\partial b}{\partial t} + u_0 \frac{\partial b}{\partial x} + N^2 w = Q(x, y, z, t) - \alpha b \tag{4}$$

$$\frac{\partial u}{\partial x} + \frac{\partial v}{\partial y} + \frac{\partial w}{\partial z} = 0, \tag{5}$$

where $u$, $v$, and $w$ are wind components in the $x$, $y$, and $z$ directions. The term $b$ is the buoyancy, $\phi$ is the geopotential, $f$ is the Coriolis parameter, $\alpha^{-1}$ ($\sim O(T_0)$, Dalu et al. 1989) is the damping timescale of Rayleigh friction (momentum and heat dissipation; Hsu 1987), and $N$ is the Brunt–Väisälä frequency. Term $Q$ is the buoyancy source (the time rate of change of the acceleration of parcel forced by the air density difference) due to the turbulent sensible heat flux, $H_t$,

$$Q = -\frac{g}{\rho C_P \theta_0} \frac{\partial H_t}{\partial z}, \tag{6}$$

where $\rho$ is the air density, $\theta_0$ is the constant reference potential temperature, $C_P$ is the heat capacity of the air at the constant pressure, and $g$ is the gravitational acceleration.

### b. Statistical description of the diabatic heating

Consider a mesoscale domain covered by a variety of vegetation or wet and dry patches of irregular patterns whose dimensions are small relative to the domain size. This situation allows the turbulent sensible heat flux (diabatic heating), $H_t$, at the surface to be modeled as a two-dimensional homogeneous random field. Here $H_t$ is further assumed to decay upward in an exponential fashion with a constant $e$-folding height $h$ ($\sim$1 km). This vertical profile of $H_t$ has been also represented by a straight line within the convective boundary layer. The use of exponential functions has advantages for the theoretical framework presented in this paper: capturing the fundamental feature of the reality (turbulent sensible heat flux decaying upward with certain scale) and mathematical simplicity essential to illuminate the rationale of the underlying physics and make the analytical solution feasible. This exponential function has been used in the theoretical study by Rotunno (1983) and is qualitatively consistent with numerical simulations of turbulent heat flux (e.g., Avissar and Chen 1993; Lynn et al. 1995b). We found that the quanti-

tative properties of the mesoscale circulation and fluxes do not sensitively depend on the shape of the vertical profile of $H_t$. (The results are available, but not presented here.) The heat flux $H_t$ has a diurnal cycle following closely the insolation curve $I(t)$. This is due to the fact that the turbulent heat flux is almost in-phase with solar radiation as corroborated by many observational studies (e.g., Smith et al. 1992). Therefore, $H_t$ is modeled as

$$H_t = \hat{H}(x, y) \exp\left(-\frac{z}{h}\right) I(t), \tag{7}$$

where $\hat{H}$ (W m$^{-2}$) is a random function characterizing the thermal variability of land surface that will be specified in section 3. Hence the buoyancy source $Q$ due to $H_t$ can be written in terms of

$$Q = \hat{Q}(x, y) \exp\left(-\frac{z}{h}\right) I(t), \tag{8}$$

where $\hat{Q}$ (m s$^{-3}$) relates to $\hat{H}$ through

$$\hat{Q} = \frac{g}{\rho C_P \theta_0 h} \hat{H}. \tag{9}$$

Assuming $\hat{H} \sim 10^2$ W m$^{-2}$, $\theta_0 \sim 300$ K, and $h \sim 10^3$ m leads to $\hat{Q}$ being on the order of $10^{-5}$ m s$^{-3}$.

The insolation curve $I(t)$ is defined by

$$I(t) = \begin{cases} \sin(\Omega t), & 0 \leq t \leq T_0/2 \text{ (daytime)} \\ 0, & T_0/2 < t \leq T_0 \text{ (night)}, \end{cases} \tag{10}$$

where $\Omega$ is the rotation rate of the earth, and $T_0$ is one day.

## 3. Analytical solution

### a. Decomposition and the spectral representation

Randomness in the buoyancy source $Q$ makes all dependent variables in Eqs. (1) through (5) random. Given the linearity of the governing equations it is safe to assume that if the external forcing of the flow is homogeneous horizontally so will be the dependent variables.

The first step in the solution of the system of stochastic differential equations is to decompose the dependent variables and the buoyancy source into their horizontal domain mean and a perturbation term around the mean:

$$u = \bar{u} + u' \tag{11}$$

$$v = \bar{v} + v' \tag{12}$$

$$w = \bar{w} + w' \tag{13}$$

$$\phi = \bar{\phi} + \phi' \tag{14}$$

$$b = \bar{b} + b' \tag{15}$$

$$\hat{Q} = \bar{\hat{Q}} + \hat{Q}'. \tag{16}$$

The linear dynamic system for the state variables $u$, $v$, $w$, $b$, and $\phi$ also implies that the perturbation terms $(\ )'$ are decoupled from the mean $\bar{(\ )}$. They both satisfy the governing Eqs. (1) through (5). From now on we focus only on the perturbation terms.

Using spectral representation (Yaglom 1987), the perturbation terms $u'$, $v'$, $w'$, $b'$, $\phi'$, and $\hat{Q}'$ can be expressed as

$$u' = \int_{-\infty}^{\infty}\int_{-\infty}^{\infty} e^{i(k_1 x + k_2 y)} dZ_u(k_1, k_2; z, t) \tag{17}$$

$$v' = \int_{-\infty}^{\infty}\int_{-\infty}^{\infty} e^{i(k_1 x + k_2 y)} dZ_v(k_1, k_2; z, t) \tag{18}$$

$$w' = \int_{-\infty}^{\infty}\int_{-\infty}^{\infty} e^{i(k_1 x + k_2 y)} dZ_w(k_1, k_2; z, t) \tag{19}$$

$$b' = \int_{-\infty}^{\infty}\int_{-\infty}^{\infty} e^{i(k_1 x + k_2 y)} dZ_b(k_1, k_2; z, t) \tag{20}$$

$$\phi' = \int_{-\infty}^{\infty}\int_{-\infty}^{\infty} e^{i(k_1 x + k_2 y)} dZ_\phi(k_1, k_2; z, t) \tag{21}$$

$$\hat{Q}' = \int_{-\infty}^{\infty}\int_{-\infty}^{\infty} e^{i(k_1 x + k_2 y)} dZ_Q(k_1, k_2), \tag{22}$$

where $dZ_u$, $dZ_v$, $dZ_w$, $dZ_b$, $dZ_\phi$, and $dZ_Q$ are the random variables in the frequency domain $(k_1, k_2)$ corresponding to $u'$, $v'$, $w'$, $b'$, $\phi'$, and $\hat{Q}'$ in the physical domain $(x, y)$. Here $dZ_Q$ has a prescribed spectral density function, $S_Q(k_1, k_2)$, characterizing the thermal variability of the land surface

$$\sigma_Q^2 S_Q(k_1, k_2) = \frac{E[|dZ_Q(k_1, k_2)|^2]}{dk_1 dk_2}, \tag{23}$$

where $\sigma_Q$ is proportional to $\sigma_H$ according to (9). Here $\sigma_H$ is the standard deviation of the turbulent heat flux into the atmosphere at the time of maximum solar radiation at the ground. It is a measure of the variability in the turbulent sensible heat flux from the land surface.

### b. Governing equations in the frequency domain

The governing equations for $dZ$ can be readily derived by substituting Eqs. (17) through (22) into Eqs. (1) through (5), resulting in

$$\left(\frac{\partial}{\partial t} + \alpha + ik_1 u_0\right)(dZ_u) - f(dZ_v) = -ik_1(dZ_\phi) \tag{24}$$

$$\left(\frac{\partial}{\partial t} + \alpha + ik_1 u_0\right)(dZ_v) + f(dZ_u) = -ik_2(dZ_\phi) \tag{25}$$

$$\left(\frac{\partial}{\partial t} + \alpha + ik_1 u_0\right)(dZ_w) - (dZ_b) = -\frac{\partial}{\partial z}(dZ_\phi) \tag{26}$$

$$\left(\frac{\partial}{\partial t} + \alpha + ik_1u_0\right)(dZ_b) + N^2(dZ_w) = I(t)\exp\left(-\frac{z}{h}\right)(dZ_Q) \quad (27)$$

$$ik_1(dZ_u) + ik_2(dZ_v) + \frac{\partial}{\partial z}(dZ_w) = 0. \quad (28)$$

*c. Solution for the dZs*

The analytical solution of the Eqs. (24) through (28) with the proper initial and boundary conditions is shown below, while the detailed derivation is given in appendix B.

1) When $N \neq f$,

$$dZ_u = i\left\{\frac{fk_2h}{f^2 - k^2h^2N^2}\left[\exp\left(-\frac{z}{h}\right) - \frac{N}{f}kh\exp\left(-\frac{N}{f}kz\right)\right]I_0(t;u_0,\alpha) - \frac{2}{\pi}\frac{kh}{1-k^2h^2}\int_a^b \cos(zkG(\xi))G(\xi)\frac{\xi k_1hI_s(t,\xi;u_0,\alpha) - fk_2hI_c(t,\xi;u_0,\alpha)}{(\Lambda^2-\xi^2)\xi}d\xi\right\}dZ_Q \quad (29)$$

$$dZ_v = -i\left\{\frac{fk_1h}{f^2 - k^2h^2N^2}\left[\exp\left(-\frac{z}{h}\right) - \frac{N}{f}kh\exp\left(-\frac{N}{f}kz\right)\right]I_0(t;u_0,\alpha) + \frac{2}{\pi}\frac{kh}{1-k^2h^2}\int_a^b \cos(zkG(\xi))G(\xi)\frac{\xi k_2hI_s(t,\xi;u_0,\alpha) + fk_1hI_c(t,\xi;u_0,\alpha)}{(\Lambda^2-\xi^2)\xi}d\xi\right\}dZ_Q \quad (30)$$

$$dZ_w = -\left\{\frac{2}{\pi}\frac{k^2h^2}{1-k^2h^2}\int_a^b \sin(zkG(\xi))\frac{I_s(t,\xi;u_0,\alpha)}{\Lambda^2-\xi^2}d\xi\right\}dZ_Q \quad (31)$$

$$dZ_b = \left\{\left[\exp\left(-\frac{z}{h}\right) + \frac{k^2h^2N^2}{f^2-k^2h^2N^2}\left(\exp\left(-\frac{z}{h}\right) - \exp\left(-\frac{N}{f}kz\right)\right)\right]I_0(t;u_0,\alpha) - \frac{2}{\pi}\frac{k^2h^2N^2}{1-k^2h^2}\int_a^b \sin(zkG(\xi))\frac{I_c(t,\xi;u_0,\alpha)}{(\Lambda^2-\xi^2)\xi}d\xi\right\}dZ_Q \quad (32)$$

$$dZ_\phi = h\left\{\frac{-f^2}{f^2-k^2h^2N^2}\left[\exp\left(-\frac{z}{h}\right) - \frac{N}{f}kh\exp\left(-\frac{N}{f}kz\right)\right]I_0(t;u_0,\alpha) + \frac{2}{\pi}\frac{kh}{1-k^2h^2}\int_a^b \cos(zkG(\xi))G(\xi)\frac{\xi^2-f^2}{\Lambda^2-\xi^2}\frac{I_c(t,\xi;u_0,\alpha)}{\xi}d\xi\right\}dZ_Q. \quad (33)$$

2) When $N = f$,

$$dZ_u = \frac{i}{f(1-k^2h^2)}\left\{\exp\left(-\frac{z}{h}\right) - kh\exp(-zk)\right\}\{k_1hI_s(t,f;u_0,\alpha) + k_2h[I_0(t;u_0,\alpha) - I_c(t,f;u_0,\alpha)]\}dZ_Q \quad (34)$$

$$dZ_v = \frac{i}{f(1-k^2h^2)}\left\{\exp\left(-\frac{z}{h}\right) - kh\exp(-zk)\right\}\{k_2hI_s(t,f;u_0,\alpha) - k_1h[I_0(t;u_0,\alpha) - I_c(t,f;u_0,\alpha)]\}dZ_Q \quad (35)$$

$$dZ_w = -\frac{k^2h^2}{f(1-k^2h^2)}\left\{\exp\left(-\frac{z}{h}\right) - \exp(-kz)\right\}I_s(t,f;u_0,\alpha)dZ_Q \quad (36)$$

$$dZ_b = \left\{\exp\left(-\frac{z}{h}\right)I_0(t;u_0,\alpha) + \frac{k^2h^2}{1-k^2h^2}\left[\exp\left(-\frac{z}{h}\right) - \exp(-zk)\right][I_0(t;u_0,\alpha) - I_c(t,f;u_0,\alpha)]\right\}dZ_Q \quad (37)$$

$$dZ_\phi = -\frac{h}{1-k^2h^2}\left\{\exp\left(-\frac{z}{h}\right) - kh\exp(-zk)\right\}I_0(t;u_0,\alpha)dZ_Q, \quad (38)$$

where

$$[a, b] = [\min\{f, N\}, \max\{f, N\}] \quad (39)$$

$$\Lambda^2 = \frac{f^2 - k^2h^2N^2}{1 - k^2h^2} \quad (40)$$

$$G(\xi) = \left| \frac{N^2 - \xi^2}{f^2 - \xi^2} \right|^{1/2} \quad (41)$$

$$I_0(t; u_0, \alpha) = \int_0^t I(\tau) \exp[-(\alpha + ik_1u_0)(t - \tau)]d\tau \quad (42)$$

$$I_s(t, \xi; u_0, \alpha) = \int_0^t I(\tau) \sin[\xi(t - \tau)] \times \exp[-(\alpha + ik_1u_0)(t - \tau)]d\tau \quad (43)$$

$$I_c(t, \xi; u_0, \alpha) = \int_0^t I(\tau) \cos[\xi(t - \tau)] \times \exp[-(\alpha + ik_1u_0)(t - \tau)]d\tau. \quad (44)$$

The term $\xi$ is a dummy integration variable, and $I(t)$ is given in (10). The other symbols are specified in appendix A.

For the sake of brevity, we rewrite the solution given in (29) through (38) as

$$dZ_u = \Pi_u(k_1, k_2; z, t)dZ_Q \quad (45)$$

$$dZ_v = \Pi_v(k_1, k_2; z, t)dZ_Q \quad (46)$$

$$dZ_w = \Pi_w(k_1, k_2; z, t)dZ_Q \quad (47)$$

$$dZ_b = \Pi_b(k_1, k_2; z, t)dZ_Q \quad (48)$$

$$dZ_\phi = \Pi_\phi(k_1, k_2; z, t)dZ_Q. \quad (49)$$

## 4. Statistics of the mesoscale circulation

In the framework of stochastic analysis the *intensity* of the mesoscale circulation can be quantified by the standard deviation (square root of the variance) $\sigma_u$, $\sigma_v$, and $\sigma_w$ of the wind velocities $u$, $v$, and $w$, respectively. They characterize the magnitude of the perturbation in wind velocities. The *horizontal distribution* of the mesoscale circulation can be characterized by the length scales. For instance, the length scale of vertical velocity $w$ provides a measure of the size of a typical circulation cell. In the frequency domain these length scales correspond to wavenumbers around which a large portion of the variance concentrates. The length scale $L$ is equal to the inverse of the wavenumber $k$ multiplied by $2\pi$.

### a. *Properties of* $\sigma_i$

The flow intensity is basically determined by the parameters characterizing the synoptic environment and the thermal properties of the landscape. Significant land-breeze circulation is expected to be associated with a sufficiently large thermal gradient. Atmospheric stability provides a resistance against the upward motion of the air forced by diabatic heating. Strong synoptic wind tends to smooth out the locally generated flow structures. The analytical solution in the previous section enables us to investigate the effects of these parameters quantitatively.

The variances can be computed from Eqs. (45) through (47) as

$$\sigma_i^2(z, t) = \int_{-\infty}^{\infty}\int_{-\infty}^{\infty} E[|dZ_i|^2]dk_1dk_2 = \int_{-\infty}^{\infty}\int_{-\infty}^{\infty} |\Pi_i(k_1, k_2; z, t)|^2\sigma_Q^2 \times S_Q(k_1, k_2)dk_1dk_2, \quad (50)$$

where the index $i$ represents $u$, $v$, $w$. This equation predicts a linear relationship between the flow intensity $\sigma_i$ and the thermal gradient $\sigma_Q$ or $\sigma_H$. In the following analysis it is convenient to normalize $\sigma_i$ by $\sigma_H$.

To compute $\sigma_i$ using (50), the functional form of $S_Q(k_1, k_2)$ needs to be specified. In principle $S_Q(k_1, k_2)$ must be estimated from the measurement of sensible heat flux at the surface over the region of interest. For the purpose of illustration we may use a hypothetical $S_Q$ function of uniform distribution over a finite frequency domain. The study by André et al. (1990) showed that nonhomogeneous landscape with characteristic horizontal scale smaller than 10 km induces no apparent coherent atmospheric response. This result suggests a higher wavenumber cutoff in $S_Q$. The lower wavenumber cutoff should correspond to a length scale not too large compared to the mesoscale domain size (~500 km). Otherwise the assumption of homogeneity of the random field of surface heating could be invalid. Based on the above considerations, the thermal variability is assumed to have the length scale ranging from 20 to 50 km, imposing a high and a low wavenumber cutoff in the $(k_1, k_2)$ domain.

First we investigate the role of synoptic wind $u_0$ on $\sigma_i$ under the conditions of neutral stratification ($N = 0$). Vertical distributions of $\sigma_u$, $\sigma_v$, and $\sigma_w$ are plotted in Fig. 1. Their time behavior is illustrated in Fig. 2. Comparing $\sigma_i$ with $u_0 = 0$ in Fig. 1 with that with $u_0 = 5$ m s$^{-1}$ in Fig. 3, we see the presence of the synoptic wind strongly inhibits the development of the flow. Here $\sigma_i$ decreases by a factor of 30 as the synoptic wind $u_0$ increases from 0 to 5 m s$^{-1}$. Hence, in an environment with moderate to strong synoptic wind the mesoscale circulation driven by the differential surface heating is very weak.

Stable stratification of the atmosphere affects not only the flow intensity but also the height below which the thermally induced air flow is active. Figure 4 shows that $\sigma_u$ and $\sigma_v$ decrease by a factor of 10 as $N$ increases

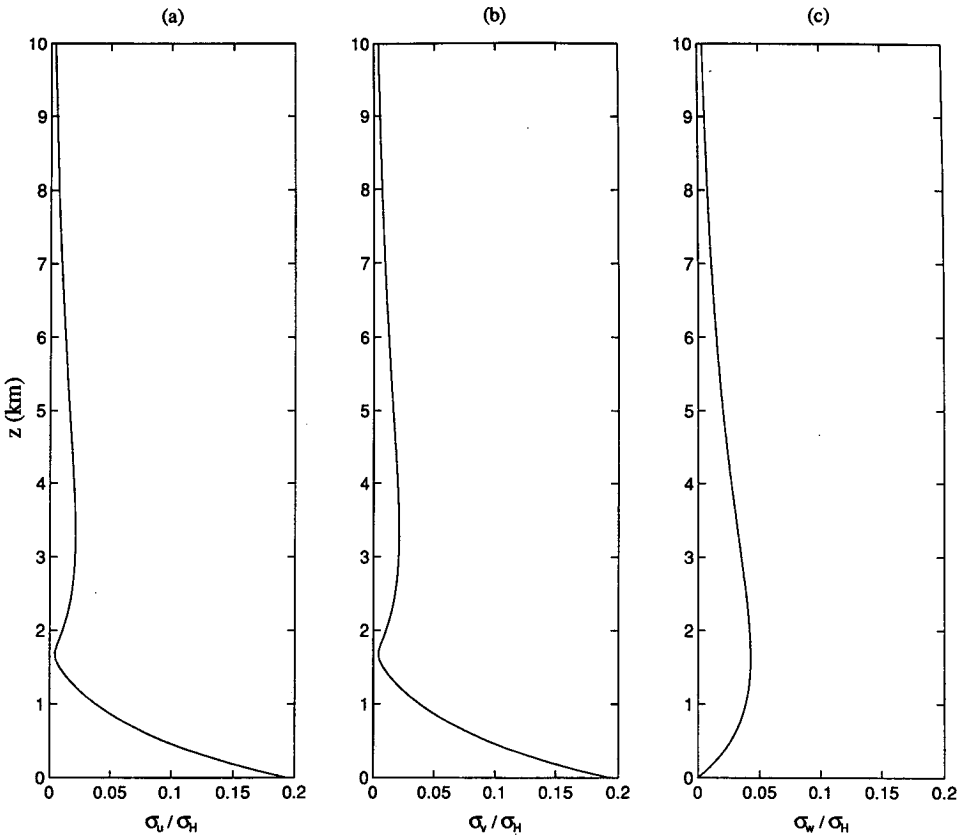


FIG. 1. Vertical profiles of standard deviation of wind velocities (a) $\sigma_u$, (b) $\sigma_v$, and (c) $\sigma_w$ (m s$^{-1}$) normalized by $\sigma_H$ (W m$^{-2}$) in the case of $N = 0$, $u_0 = 0$ and $\alpha = 1.2\Omega$ at $t = 1500$ LT.

from 0 to $10^{-2}$ s$^{-1}$. At the same time $\sigma_w$ decreases by a factor of 200! Also the height of $\sigma_w^{\max}$ moves from 1800 m down to about 200 m. The flow in such an environment is constrained within a shallow layer near the surface. The stable atmosphere substantially reduces the intensity and the vertical range of the mesoscale circulation. Consequently, the associated mesoscale fluxes of momentum, heat, and moisture are also suppressed.

Rayleigh friction affects both intensity and structure of the mesoscale circulation. As $\alpha$ decreases from $1.2\Omega$ to zero, the intensity of the flow will increase by a factor of three. Without the dissipation ($\alpha = 0$) our results show a nonphysical second circulation peak during the nighttime when there is no solar radiation. These results are not presented.

Comparing Figs. 1, 2, and 3 with Figs. 3 and 8 in Avissar and Chen (1993), we find that general features of the distributions of the horizontal mean mesoscale kinetic energy per unit mass (MKE), $(\sigma_u^2 + \sigma_v^2)/2$, predicted by this stochastic linear theory are consistent with those obtained using the sophisticated mesoscale numerical model. For example, their numerical simulations show that the peak MKE occurs at about 1500 LT. Our theory (see Fig. 2) gives the same result. We note that MKE is zero at $z = 0$ in the numerical simulations, while nonzero from our theory. This difference is caused by the boundary conditions. In the turbulent atmospheric circulation model wind speed at the ground usually is set to be zero because of viscosity. In our linear theory the effect of viscosity is neglected.

We conclude that stability $N$ and synoptic wind $u_0$ significantly inhibit the development of the mesoscale circulation caused by the thermal inhomogeneity of the landscape. The flow will not develop to a significant level except in a synoptic environment characterized by a neutral stratification and weak synoptic wind.

### *b. Properties of the spatial length scale*

The length scale of the thermally induced mesoscale circulation will be studied by analyzing the frequency response function (a term borrowed from system analysis) $\Pi_i$ in Eqs. (45)–(47). The frequency response function fully characterizes the input–output relation of a linear dynamic system when the power is decomposed over frequencies. For the case of zero synoptic wind, $\Pi_w$ depends only on the radius wavenumber $k$, implying an isotropic field of vertical velocity $w$. Hence the scale analysis of the flow is facilitated by studying the properties of $\Pi_w$ for $u_0 = 0$.

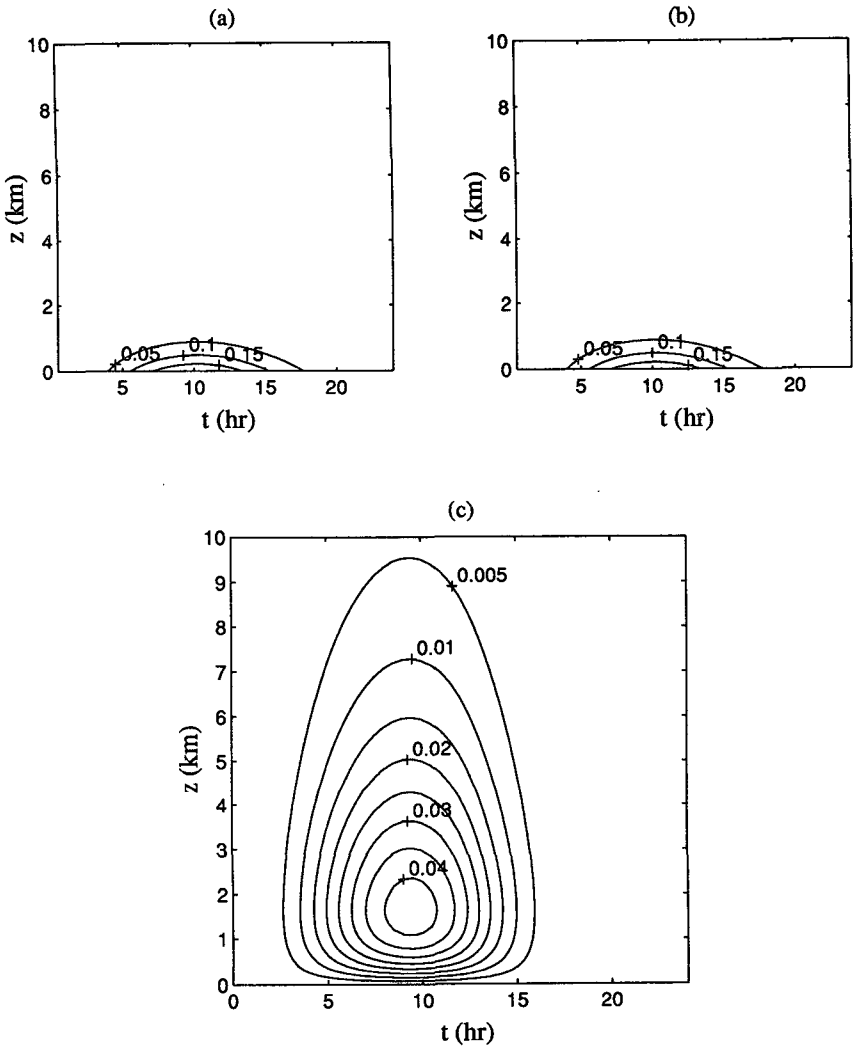


FIG. 2. The $z$–$t$ distribution of (a) $\sigma_u/\sigma_H$, (b) $\sigma_v/\sigma_H$, and (c) $\sigma_w/\sigma_H$ with $N = 0$, $u_0 = 0$, and $\alpha = 1.2\Omega$. Here $t$ is the time after sunrise.

A common feature of $\Pi_w$ for all altitudes is that it goes to zero as wavenumber $k$ goes to zero (Fig. 5). This means the thermal heterogeneity with sufficiently large-scale $L$ (very small thermal gradient) is inefficient in driving the land-breeze-type flow in the 3D domain. On the other hand, $\Pi_w$ behaves differently as a function of wavenumber $k$ at different altitudes. At low altitude, for example $z = 0.1$ km, $\Pi_w$ (Fig. 5) initially increases with the wavenumber $k$, then saturates at $k \approx 50$, corresponding to a length scale $L \approx 0.1$ km. At $z = 1$ km, $\Pi_w$ behaves similarly but the saturation point moves from $k \approx 50$ down to $k \approx 5$. Consequently the corresponding length scale $L$ increases from 0.1 km to about 1 km. Hence at relatively low altitude the atmosphere has little response to the thermal forcing with large length scales. However, at higher altitudes, $\Pi_w$ reaches a maximum at certain finite wavenumber, $k_{\max}$. With increasing altitude, the peak of $\Pi_w$ becomes sharper, and $k_{\max}$ becomes smaller. The atmosphere is most sensitive to the thermal forcing at this particular wavenumber $k_{\max}$. This behavior could be interpretated as a resonance phenomenon in many dynamic systems. Mesoscale circulation is likely to be observed when the length scale of the forcing is close to the inherent length scale of the mesoscale system. Due to the rapid decay of diabatic heating upward, the forcing needs to be more concentrated around this inherent scale of the mesoscale system so that the mesoscale flow can be driven to a deeper depth. The graph in Fig. 5b shows the dependence of $k_{\max}$ on altitude $z$. The $L_{\max} - z$ relation is plotted in Fig. 6.

The dependence of $\Pi_u$, $\Pi_v$, and $\Pi_b$ on $k$ turns out to be similar to that of $\Pi_w$ except that they vanish as $k$ goes to infinity. There exist certain wavenumbers (or

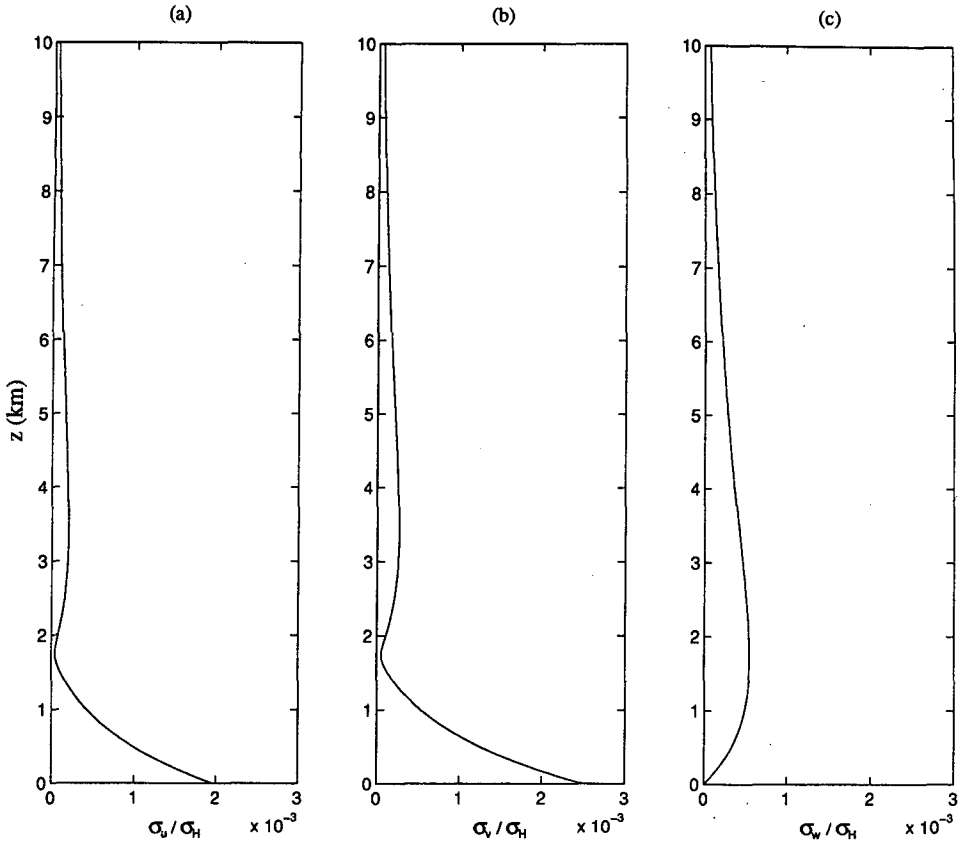


FIG. 3. Same as Fig. 1 except $u_0 = 5$ m s$^{-1}$.

length scales) at which these $|\Pi|$ functions have peaks. This property implies that the land-surface heterogeneity at certain scales is most effective in driving the mesoscale circulation and fluxes. Influences of landscape variability at very large as well as very small scales on the mesoscale circulation are minimum according to our stochastic linear theory.

In summary, the atmosphere at lower altitude responds to the thermal forcing with small length scales, while at higher altitude it tends to be driven by the forcing with large length scale.

## 5. Water balance in the atmosphere

### a. Governing equations

As a first-order approximation we ignore the effect of the latent heat released by the condensation of the water vapor on the atmospheric flow. Thus moisture is assumed to be a passive tracer. The water balance in the atmosphere without precipitation simply states that the total water content $q$ (kg kg$^{-1}$) is conserved following the flow:

$$\frac{\partial q}{\partial t} + \frac{\partial}{\partial x}(uq) + \frac{\partial}{\partial y}(vq) + \frac{\partial}{\partial z}(wq) = 0, \quad (51)$$

where $u$, $v$, and $w$ are the 3D wind velocities described by Eqs. (1) through (5).

Using the same arguments as for $u$, $v$, $w$, $b$, and $\phi$, the random field $q$ is assumed homogeneous horizontally. As we did in section 3a, $q$ is decomposed into the domain mean $\bar{q}$ and the perturbation term $q'$

$$q = \bar{q} + q', \quad (52)$$

where $q'$ is expressed with the aid of the spectral representation of homogeneous random field as

$$q' = \int_{-\infty}^{\infty}\int_{-\infty}^{\infty} e^{i(k_1 x + k_2 y)} dZ_q(k_1, k_2; z, t). \quad (53)$$

The governing equation for $q'$ can be derived by linearizing Eq. (51). The detailed derivation is shown in appendix C. We have

$$\frac{\partial q'}{\partial t} + u_0 \frac{\partial q'}{\partial x} + w' \frac{d\bar{q}}{dz} = 0, \quad (54)$$

where $\bar{q}$ is the mean vertical profile of the moisture in the atmosphere.

The governing equation for $dZ_q$ in the frequency domain is obtained by substituting Eq. (53) into Eq. (54):

$$\frac{\partial}{\partial t}(dZ_q) + ik_1 u_0 (dZ_q) = -\frac{d\bar{q}(z)}{dz} dZ_w. \quad (55)$$

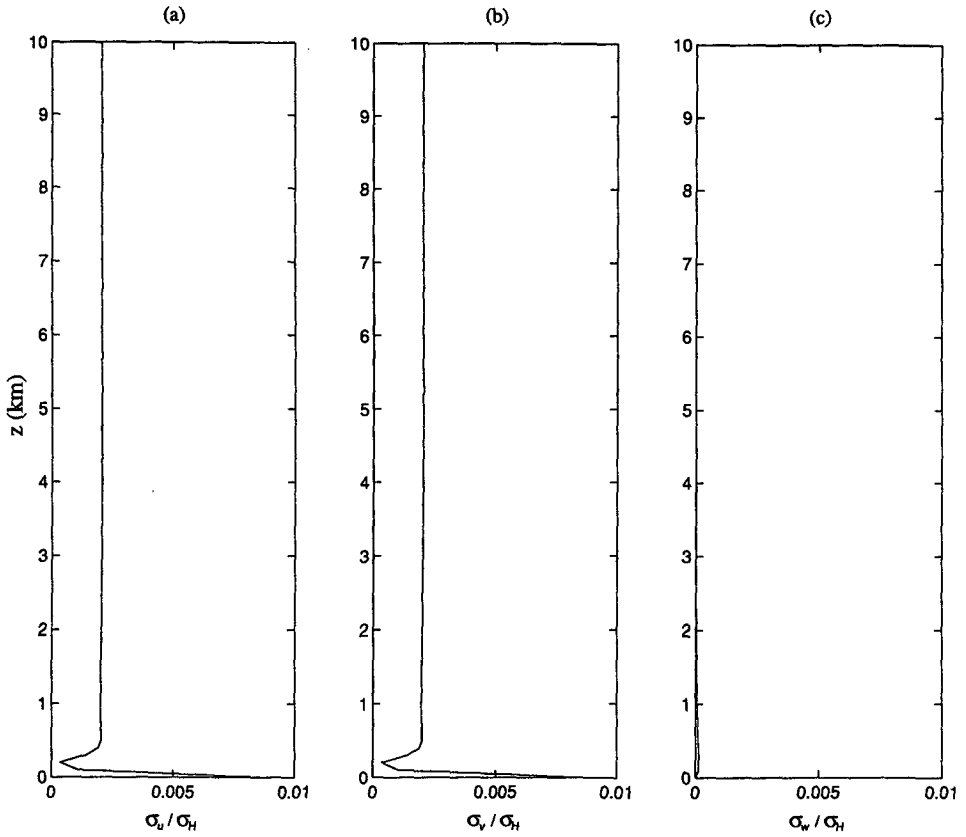


FIG. 4. Same as Fig. 1 except $N = 10^{-2}\ s^{-1}$.

*b. Analytical solution*

Analogous to the procedure used in appendix B for the solution of $dZ_u$, $dZ_v$, $dZ_w$, $dZ_b$, and $dZ_\phi$, the analytical solution of $dZ_q$ can be shown as follows.

1) When $N \neq f$,

$$dZ_q = \frac{d\bar{q}(z)}{dz}\left\{\frac{k^2h^2}{(f^2+\alpha^2)-k^2h^2(N^2+\alpha^2)}\left[\exp\left(-\frac{z}{h}\right)-\exp(-kz(N^2+\alpha^2)^{1/2}(f^2+\alpha^2)^{-1/2})\right]\right.$$
$$\left.\times I_0(t;u_0,0)-\frac{2}{\pi}\frac{k^2h^2}{1-k^2h^2}\int_a^b \sin(zkG(\xi))\frac{\xi I_c(t,\xi;u_0,\alpha)+\alpha I_s(t,\xi;u_0,\alpha)}{(\Lambda^2-\xi^2)(\xi^2+\alpha^2)}\,d\xi\right\}dZ_Q. \quad (56)$$

2) When $N = f$,

$$dZ_q = \frac{d\bar{q}(z)}{dz}\left\{\frac{k^2h^2}{(f^2+\alpha^2)(1-k^2h^2)}\left[\exp\left(-\frac{z}{h}\right)-\exp(-zk)\right]\right.$$
$$\left.\times\left[I_0(t;u_0,0)-I_c(t,f;u_0,\alpha)-\frac{\alpha}{f}I_s(t,f;u_0,\alpha)\right]\right\}dZ_Q. \quad (57)$$

Again, we write (56) and (57) in a short form

$$dZ_q = \frac{d\bar{q}(z)}{dz}\Pi_q(k_1,k_2;z,t)dZ_Q. \quad (58)$$

## 6. Mesoscale fluxes

Many recent numerical studies have argued that heat fluxes associated the thermally induced flow may be

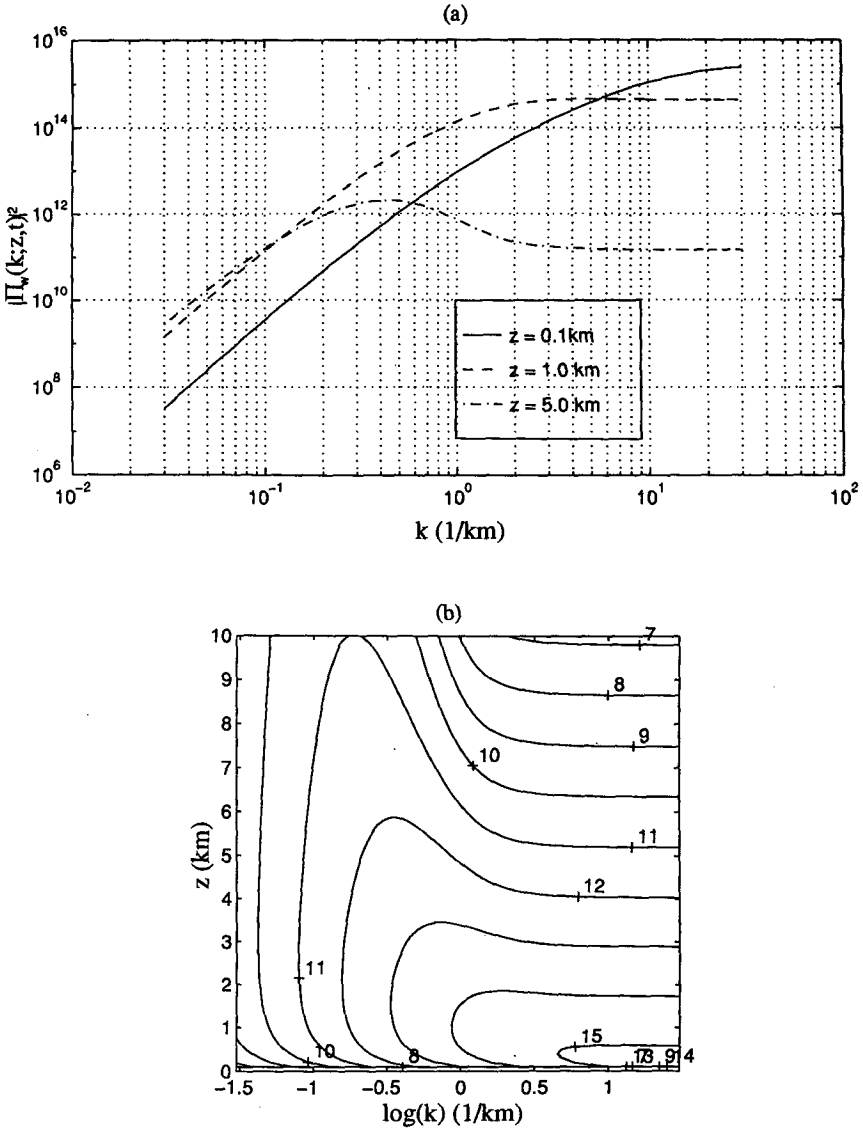


FIG. 5. (a) The $k$ dependence of $|\Pi_w(k; z, t)|^2$ at $z = 0.1$-, 1.0-, and 5.0-km altitude and (b) $z - \log k$ distribution of $\log(|\Pi_w|^2)$ for $N = 0$, $u_0 = 0$, and $\alpha = 1.2\Omega$ at $t = 1500$ LT.

comparable to the turbulent heat fluxes under the same synoptic conditions. Next we attempt to study the intensity and the spatial–temporal patterns of the mesoscale fluxes of momentum, heat, and moisture using the analytical solutions obtained in the previous section.

Mesoscale vertical fluxes of momentum $M_m^x$ and $M_m^y$, sensible heat $H_m$, and moisture $E_m$ are defined by Avissar and Chen (1993) and Lynn et al. (1995b) as

$$M_m^x = \overline{w'u'} \tag{59}$$

$$M_m^y = \overline{w'v'} \tag{60}$$

$$H_m = \overline{w'\theta'} \tag{61}$$

$$E_m = \overline{w'q'}, \tag{62}$$

where the overbar represents (horizontal) domain average, and $\theta'$ is related to buoyancy $b'$ in the following way

$$\theta' = \frac{\theta_0}{g} b'.$$

In the frequency domain, this relation is

$$dZ_\theta = \frac{\theta_0}{g} dZ_b.$$

Using the analytical solution of $dZ$s given in section 3c, these domain-averaged primed terms can be replaced by the ensemble mean in the frequency domain $(k_1, k_2)$ using Eqs. (45) through (48):

$$M_m^x(z,t) = \int_{-\infty}^{\infty}\int_{-\infty}^{\infty} E[dZ_w(k_1,k_2;z,t) \times dZ_u^*(k_1,k_2;z,t)] = \int_{-\infty}^{\infty}\int_{-\infty}^{\infty} |\Pi_w(k_1,k_2;z,t) \times \Pi_u^*(k_1,k_2;z,t)|\sigma_Q^2 S_Q(k_1,k_2)dk_1dk_2 \quad (63)$$

$$M_m^y(z,t) = \int_{-\infty}^{\infty}\int_{-\infty}^{\infty} E[dZ_w(k_1,k_2;z,t) \times dZ_v^*(k_1,k_2;z,t)] = \int_{-\infty}^{\infty}\int_{-\infty}^{\infty} |\Pi_w(k_1,k_2;z,t) \times \Pi_v^*(k_1,k_2;z,t)|\sigma_Q^2 S_Q(k_1,k_2)dk_1dk_2 \quad (64)$$

$$H_m(z,t) = \int_{-\infty}^{\infty}\int_{-\infty}^{\infty} E[dZ_w(k_1,k_2;z,t) \times dZ_\theta^*(k_1,k_2;z,t)] = \int_{-\infty}^{\infty}\int_{-\infty}^{\infty} |\Pi_w(k_1,k_2;z,t) \times \Pi_\theta^*(k_1,k_2;z,t)|\sigma_Q^2 S_Q(k_1,k_2)dk_1dk_2 \quad (65)$$

$$E_m(z,t) = \int_{-\infty}^{\infty}\int_{-\infty}^{\infty} E[dZ_w(k_1,k_2;z,t) \times dZ_q^*(k_1,k_2;z,t)] = \left\{\int_{-\infty}^{\infty}\int_{-\infty}^{\infty} |\Pi_w(k_1,k_2;z,t) \times \Pi_q^*(k_1,k_2;z,t)|\sigma_Q^2 S_Q(k_1,k_2)dk_1dk_2\right\} \times \frac{d\bar{q}(z)}{dz}. \quad (66)$$

### a. *Momentum fluxes*

It has already been found using a 2D model (Dalu and Pielke 1993) that mesoscale momentum flux is zero in the absence of synoptic wind. Our 3D linear stochastic model also predicts a zero momentum flux in the absence of synoptic wind. However, in the presence of a moderate synoptic wind $u_0$ our 3D model predicts that the mesoscale momentum fluxes will no longer be zero. The vertical structure of the momentum fluxes $M_m^x$ and $M_m^y$ in the neutral atmosphere ($N = 0$) are computed from Eqs. (63) and (64) and plotted in Fig. 7a. We note that the momentum flux associated with the horizontal wind in the direction of synoptic wind $u_0$ is zero. The nonzero momentum flux is due to the horizontal wind perpendicular to the direction of the synoptic wind. This property of momentum flux is fundamentally different from that of momentum flux (if any) predicted by 2D models. Given a reasonable value of $\sigma_H \approx 50$ W m$^{-2}$ (see Fig. 4 of Lynn et al. 1995b), $M_m^y$ is on the order of $8 \times 10^{-5} \times 50^2 = 0.2$ m$^2$ s$^{-2}$, considerably larger than the typical value of the turbulent momentum flux (0.05 m$^2$ s$^{-2}$) according to Stull (1988). This significant difference between the mesoscale momentum flux and the turbulent momentum flux indicates that the transport of momentum from the synoptic flow to the locally generated mesoscale flow could be much stronger than that due to the surface friction. The evident mesoscale momentum flux also sheds some light on the interaction between the circulation at large scale and the organized flow at mesoscale. Fig. 7b shows that the strongest mesoscale momentum transport occurs in the afternoon, about 9 hours after sunrise. In the lower atmosphere, the momentum flux is downward (negative), while above a certain altitude it becomes upward (positive) as shown in Fig. 7.

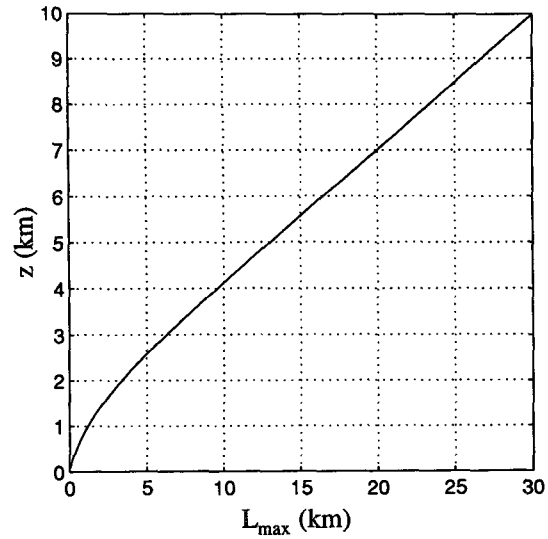


FIG. 6. Plot of $L_{\max} = 2\pi/k_{\max}$, where $k_{\max}$ is the wavenumber at which $|\Pi_w|^2$ in Fig. 5 reaches the maximum.

Based on the previous discussion, a strong synoptic wind will eventually eliminate the flow structure and consequently the momentum flux. Therefore, we expect the maximum momentum flux should be associated with a moderate value of the synoptic wind. The dependence of $M_m^y$ on $u_0$ is plotted in Fig. 8. Term $M_m^y$ increases with the synoptic wind up to $u_0 \approx 0.5$ m s$^{-1}$, then decreases at a slower rate.

Prediction of the momentum flux demonstrates one of the advantages of the 3D model. The existing 2D

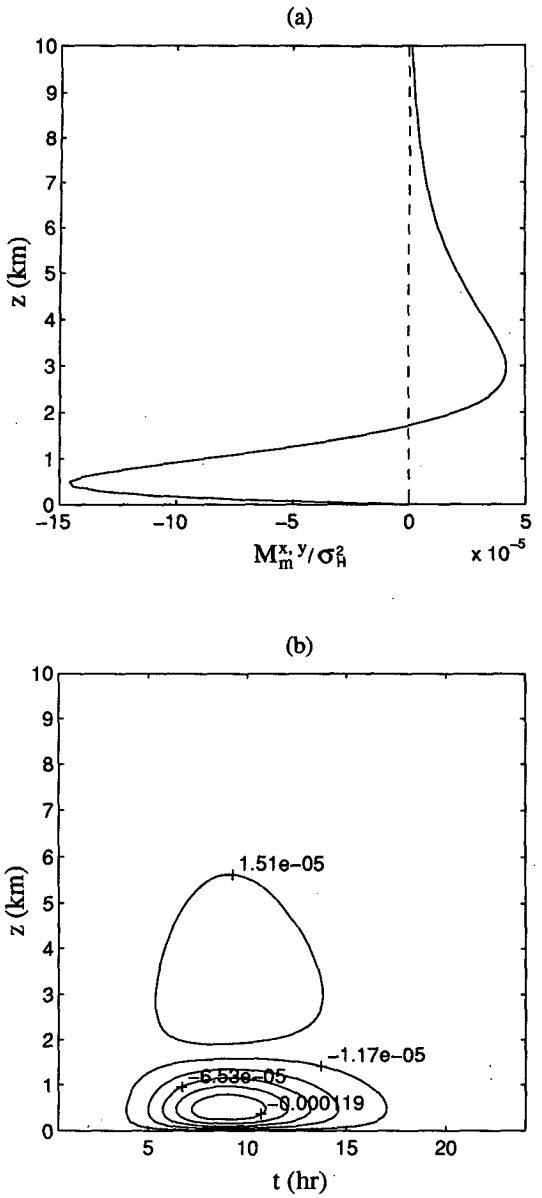


FIG. 7. (a) Vertical profiles of momentum fluxes $M_m^x/\sigma_H^2$ (dashed line) and $M_m^y/\sigma_H^2$ (solid line) at $t$ = 1500 LT and (b) $z$–$t$ distribution of $M_m^y/\sigma_H^2$ with $u_0$ = 1 m s$^{-1}$ and $\alpha = 1.2\Omega$. Here $t$ is the time after sunrise (0600 LT).

linear models may not be able to predict the existence of the momentum flux even when the synoptic wind factor is included in the governing equations because the momentum flux is caused by the wind component perpendicular to the synoptic wind. Another implication of this behavior is that prediction of momentum flux (if any) by 2D models may result from the assumption of a 2D flow configuration (always 3D in the real world) rather than from the underlying physical mechanism of the processes.

*b. Heat flux*

The vertical distribution of the mesoscale heat flux $H_m$ is plotted in Fig. 9a in the case of neutral stability and zero-synoptic wind. It can be seen that $H_m$ could be as large as the turbulent heat flux $H_t$ at the surface. Using the same value of $\sigma_H$ as above, the maximum mesoscale heat flux $H_m$ from Fig. 9b is about $50^2 \times 0.06 = 150$ W m$^{-2}$, which is comparable to the typical turbulent heat flux in the boundary layer. Figure 9b shows that the maximum $H_m$ occurs at 1500 LT.

Synoptic wind strongly inhibits the mesoscale transport of heat away from the surface. Under the condition of slight synoptic wind ($u_0$ = 1 m s$^{-1}$), $H_m$ will decrease by a factor of 10 (see Fig. 11a). Friction plays a key role in determining the structure and timing of $H_m$. Without friction, $H_m$ will be positive (upward transport of heat) until 2100 LT. Then $H_m$ becomes negative up to 0600 LT (sunrise) the next day. During this period of time, a downward transport of heat (nonphysical) is associated with the flow. This is due to the fact that there is no heat sink in the atmosphere so that the heat released from the surface accumulates.

The qualitative properties of $H_m$ are also consistent with the numerical simulations of Lynn et al. (1995b) such as the timing of the peak $H_m$ and the altitude at which $H_m$ reaches maximum. It should not be surprising to see the discrepancies in the magnitude of $H_m$ because different land-surface conditions and different parameters such as Rayleigh friction coefficient $\alpha$ are used.

*c. Moisture flux*

Equating the expression within the brackets on the right-hand side of (66) to the mesoscale moisture dif-

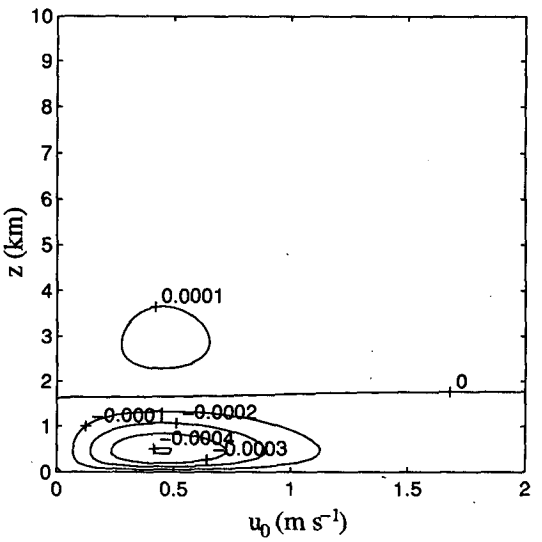


FIG. 8. Vertical distribution of momentum flux $M_m^y/\sigma_H^2$ varying with synoptic wind $u_0$, where $N = 0$, $\alpha = 1.2\Omega$ at 1500 LT or 9 hours after sunrise.

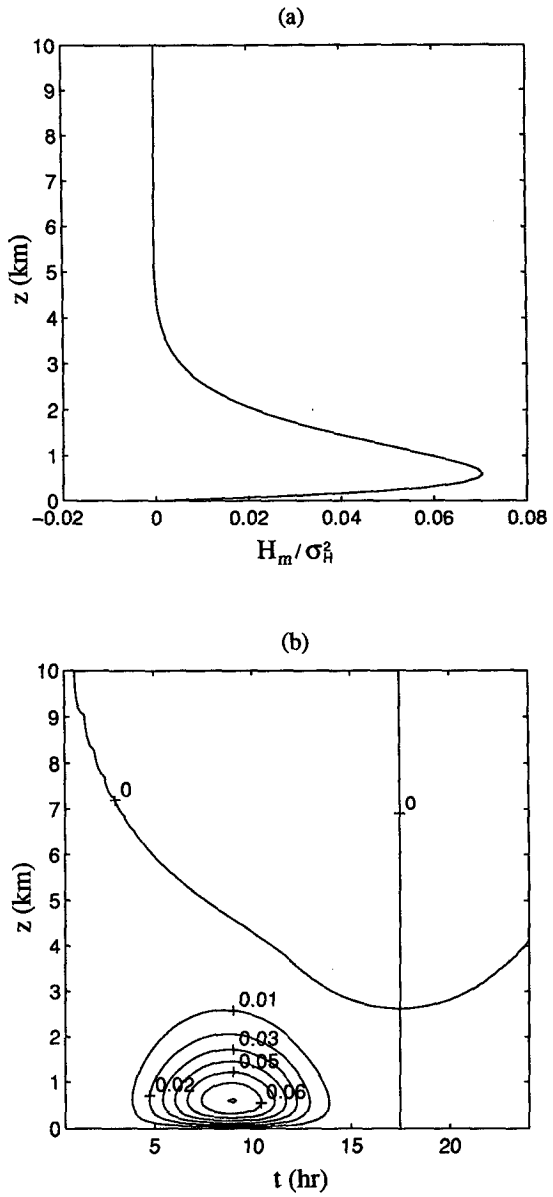


FIG. 9. (a) Vertical profile of heat flux $H_m/\sigma_H^2$ at $t$ = 1500 LT and (b) $z$–$t$ distribution of $H_m/\sigma_H^2$ in the case of $N = 0$, $u_0 = 0$, and $\alpha = 1.2\Omega$. Term $t$ is the time after sunrise (0600 LT).

fusion coefficient – $D_m(z, t)$, the mesoscale moisture flux $E_m$ can be expressed as

$$E_m = -D_m(z, t)\frac{d\bar{q}(z)}{dz}. \qquad (67)$$

Our 3D linear theory predicts that the mesoscale moisture flux is proportional to the gradient of the mean moisture distribution. This expression is formally similar to the turbulent moisture flux where the diffusion coefficient is due to the turbulent nature of the flow. However, the turbulent diffusion coefficient has to be determined from either measurements or numerical simulations because no analytical solution of turbulent flow has been found so far. The mesoscale moisture diffusion coefficient $D_m$ is obtained analytically under the linearity assumption.

The vertical structure and the $z - t$ distribution of $D_m$ is computed under the conditions of neutral stratification; zero-synoptic wind are illustrated in Figs. 10a and 10b, respectively. The impact of synoptic wind on $D_m$ is even stronger than that on $H_m$ discussed previ-

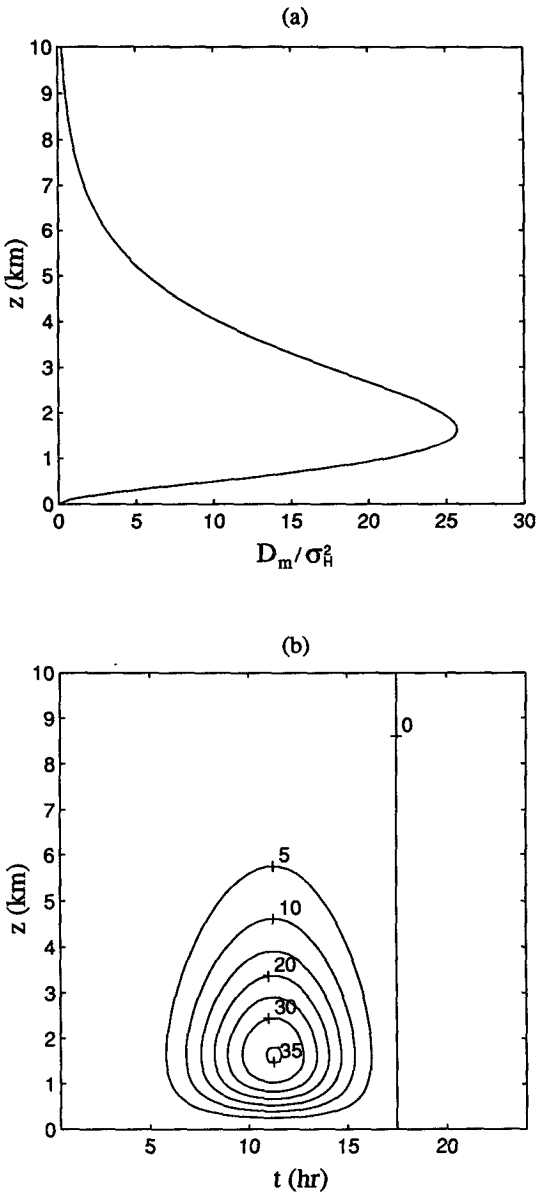


FIG. 10. (a) Vertical profile of the mesoscale diffusion coefficient $D_m/\sigma_H^2$ at $t$ = 1500 LT and (b) $z$–$t$ distribution of $D_m/\sigma_H^2$ in the case of $N = 0$, $u_0 = 0$, and $\alpha = 1.2\Omega$. Here $t$ is the time after sunrise (0600 LT).

ously. As the synoptic wind $u_0$ increases from 0 to 1 m s$^{-1}$, $D_m$ is reduced by a factor of 25 (see Fig. 11b). Notice that the maximum $D_m$ occurs at a level that is the same as that of vertical velocity (Fig. 1c) but different from that of $H_m$ (Fig. 9a). This is due to the fact that water vapor in our linear theory is a passive trace. Hence water vapor basically follows the circulation patterns characterized by the distribution of vertical velocity, $\sigma_w$. On the other hand, vertical transport of heat is determined jointly by the diabatic heating source $Q$ and the vertical velocity $w$. That is why the structures of vertical transport of heat and moisture are not identical. Here $H_m$ depends in a nonlinear way on the mean potential temperature profile characterized by $N$, while $D_m$ is independent of the mean profile of moisture, $\bar{q}(z)$, shown in Eq. (67).

Two main assumptions are inherent in deriving $E_m$ in Eq. (67): no source of moisture (e.g., soil evaporation) in the atmosphere and no precipitation by condensation. Both of them are the direct consequences of the linearization of the water balance described by Eq. (51). Therefore, this linear theory is unable to deal with the formation of cloud and rainfall that inevitably involves nonlinear analysis.

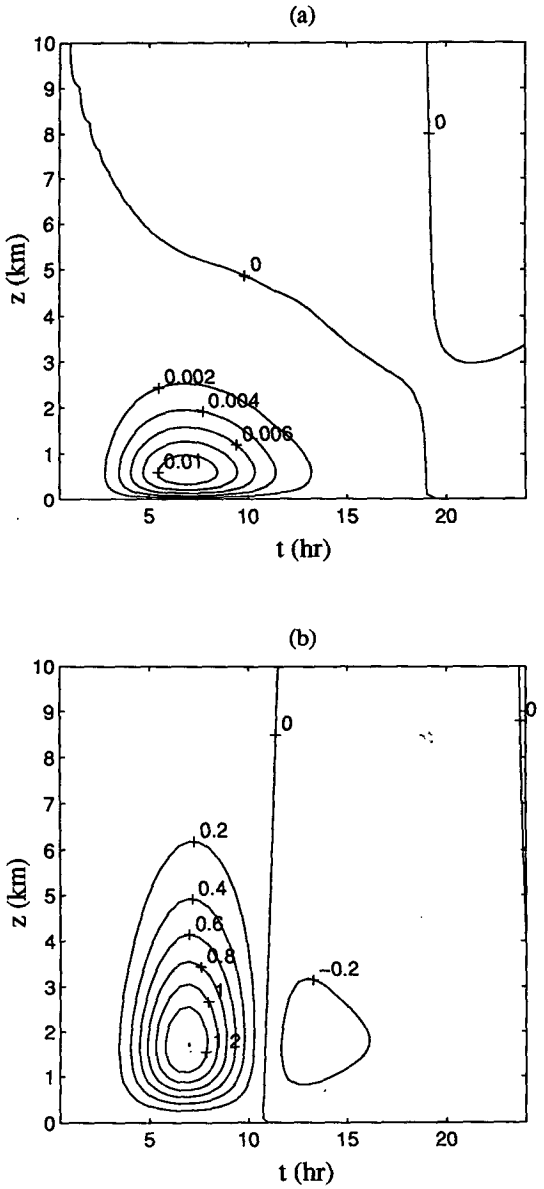


FIG. 11. (a) Same as Fig. 9b except $u_0$ = 1 m s$^{-1}$ and (b) same as Fig. 10b except $u_0$ = 1 m s$^{-1}$.

## 7. Summary and conclusions

In this paper a three-dimensional stochastic linear theory of mesoscale circulation induced by thermal heterogeneity of the land surface is developed. The equations of atmospheric flow are formulated as a set of linear stochastic partial differential equations (SPDEs) driven by randomly variable diabatic heating due to turbulent sensible heat flux from the surface. The SPDEs have been solved analytically.

The intensity of the thermally induced mesoscale circulation is shown to be proportional to the standard deviation of the turbulent sensible heat flux at the surface. In the lower atmosphere the thermal variability of landscape at smaller length scales is more efficient in triggering convection, while at higher altitudes the atmospheric dynamics are more sensitive to thermal forcing at longer length scales. The atmosphere from bottom to top behaves as a low-pass filter to the thermal variability of the landscape.

Mesoscale fluxes of momentum, heat, and moisture are found to be proportional to the variance of the turbulent sensible heat flux at the surface. It turns out that the mesoscale vertical flux of momentum is insignificant in the absence of synoptic wind. A nonzero momentum flux is associated with the presence of synoptic wind. It increases as the synoptic wind goes from zero up to a rather small value ($\sim$0.5 m s$^{-1}$) and then decreases at a slower rate. Only the flow perpendicular to the direction of synoptic wind contributes to this momentum flux. This is the reason why 2D linear models may not be able to predict a mesoscale momentum flux. We have shown, according to this linear theory, that mesoscale heat flux could be comparable, under conditions of small synoptic wind and neutral stratification, to the surface turbulent sensible flux, as found from many numerical simulations. The vertical structure of mesoscale heat flux from this 3D linear model is in good agreement with results obtained using sophisticated 3D mesoscale numerical models (e.g., Avissar and Chen 1993; Lynn et al. 1995a,b). The moisture flux predicted by this 3D linear model is proportional to the vertical gradient of mean moisture profile. The mesoscale diffusion coefficient follows the structure of flow closely since the moisture is treated as a passive tracer.

Stable stratification and synoptic wind strongly inhibit the development of the thermally induced mesoscale circulation and hence reduce drastically the associated mesoscale transport of momentum, heat, and moisture. Our results indicate that mesoscale fluxes, in this linear framework, are important only in the environments with neutral stratification and very weak synoptic wind.

Appropriate observational datasets that can be used directly to verify our theory are not currently available. The major problem with the existing datasets is that they have insufficient spatial coverage (see, e.g., Sun and Mahrt 1994) or do have sufficient spatial coverage but do not have enough spatial resolution; hence they do not meet our need. Therefore, a new field experiment is being designed and hopefully will be launched in the near future.

*Acknowledgments.* This work was supported by the National Science Foundation under Grants EAR-9120386 and ATM-9020832.

APPENDIX A

## List of Symbols

| | |
|---|---|
| $b$ | Buoyancy |
| $C_P$ | Specific heat capacity of the air at constant pressure |
| $E_m$ | Mesoscale moisture flux |
| $f$ | Coriolis parameter ($=2\Omega \sin\varphi$) |
| $H_m$ | Mesoscale sensible heat flux |
| $H_t$ | Turbulent sensible heat flux |
| $h$ | Vertical scale of diabatic heating (taken to be 1 km in this paper) |
| $i$ | Pure imaginary number $\sqrt{-1}$ |
| $k$ | Radius wavenumber $(k_1^2 + k_2^2)^{1/2}$ |
| $k_1, k_2$ | Wavenumber in $x$ and $y$ direction |
| $L$ | Length scale |
| $M_m^x, M_m^y$ | Mesoscale momentum fluxes associated with $u$ and $v$ |
| $N$ | Constant Brunt–Väisälä frequency |
| $q$ | Water content of the air |
| $Q$ | Buoyancy source due to diabatic heating |
| $r$ | Radius distance $(x^2 + y^2)^{1/2}$ |
| $S(k_1, k_2)$ | Spectral density function |
| $t$ | Time |
| $T_0$ | Length of a day (24 hours) |
| $u, v, w$ | Wind velocity in $x$, $y$, and $z$ direction |
| $u_0$ | Constant synoptic wind in $x$ direction |
| $x, y$ | Horizontal coordinates |
| $z$ | Vertical coordinate ($z$ is normalized by $h$ in all figures) |
| $\alpha$ | Inverse of linear damping timescale |
| $\theta$ | Potential temperature |
| $\rho$ | Density of air |
| $\sigma^2$ | Variance |
| $\phi$ | Geopotential |
| $\varphi$ | Latitude |
| $\Omega$ | Rotation rate of the earth ($=2\pi/T_0$) |
| $E[\ ]$ | Ensemble average (mathematical expectation) |
| $\bar{(\ )}$ | Horizontal domain average |
| $(\ )^*$ | Complex conjugate |

APPENDIX B

## Approach to the Solution

Denote the Laplace operator by $\mathcal{L}_{t,s}$, where $t$ is the independent variable that the Laplace transform refers to, $\mathcal{L}_{t,s}\{f(t)\} \equiv F(s)$. Then we may express

$$\mathcal{L}_{t,s}\{dZ_u(k_1, k_2; z, t)\} = \tilde{U}(k_1, k_2; z, s)$$
$$\mathcal{L}_{t,s}\{dZ_v(k_1, k_2; z, t)\} = \tilde{V}(k_1, k_2; z, s)$$
$$\mathcal{L}_{t,s}\{dZ_w(k_1, k_2; z, t)\} = \tilde{W}(k_1, k_2; z, s)$$
$$\mathcal{L}_{t,s}\{dZ_b(k_1, k_2; z, t)\} = \tilde{B}(k_1, k_2; z, s)$$
$$\mathcal{L}_{t,s}\{dZ_\phi(k_1, k_2; z, t)\} = \tilde{\Phi}(k_1, k_2; z, s),$$

and

$$\mathcal{L}_{z,p}\{\tilde{U}(k_1, k_2; z, s)\} = U(k_1, k_2; p, s)$$
$$\mathcal{L}_{z,p}\{\tilde{V}(k_1, k_2; z, s)\} = V(k_1, k_2; p, s)$$
$$\mathcal{L}_{z,p}\{\tilde{W}(k_1, k_2; z, s)\} = W(k_1, k_2; p, s)$$
$$\mathcal{L}_{z,p}\{\tilde{B}(k_1, k_2; z, s)\} = B(k_1, k_2; p, s)$$
$$\mathcal{L}_{z,p}\{\tilde{\Phi}(k_1, k_2; z, s)\} = \Phi(k_1, k_2; p, s).$$

Laplace transforms of Eqs. (24) through (28) with respect to $t$ lead to

$$(s + \alpha + ik_1u_0)\tilde{U} - f\tilde{V} = -ik_1\tilde{\Phi} \tag{68}$$

$$(s + \alpha + ik_1u_0)\tilde{V} + f\tilde{U} = -ik_2\tilde{\Phi} \tag{69}$$

$$(s + \alpha + ik_1u_0)\tilde{W} - \tilde{B} = -\frac{\partial\tilde{\Phi}}{\partial z} \tag{70}$$

$$(s + \alpha + ik_1u_0)\tilde{B} + N^2\tilde{W} = \tilde{I}(s)\exp\left(-\frac{z}{h}\right)dZ_Q \tag{71}$$

$$ik_1\tilde{U} + ik_2\tilde{V} + \frac{\partial\tilde{W}}{\partial z} = 0, \tag{72}$$

where, according to (10),

$$\tilde{I}(s) = \mathcal{L}_{t,s}\{I(t)\} = \frac{1}{1 - \exp(-\pi s/\Omega)}\frac{\Omega}{s^2 + \Omega^2}. \tag{73}$$

Laplace transforms of Eqs. (68) through (72) with respect to $z$ result in

$$(s + \alpha + ik_1u_0)U - fV = -ik_1\Phi \tag{74}$$

$$(s + \alpha + ik_1u_0)V + fU = -ik_2\Phi \tag{75}$$

$$(s + \alpha + ik_1u_0)W - B = -p\Phi + \tilde{\Phi}(0, s) \tag{76}$$

$$(s + \alpha + ik_1u_0)B + N^2W = \tilde{I}(s)\frac{1}{p + 1/h}dZ_Q \quad (77)$$

$$ik_1U + ik_2V + pW = \tilde{W}(0, s), \quad (78)$$

where the boundary conditions $\tilde{W}(0, s)$ and $\tilde{\Phi}(0, s)$ are determined such that all the perturbation terms vanish as the vertical coordinate $z$ goes to infinity and vertical velocity $w$ is zero at the ground:

$$\lim_{z\to\infty} u', v', w', b', \phi' = 0 \quad (79)$$

$$w'|_{z=0} = 0. \quad (80)$$

Performing Laplace transform twice converts the original partial differential Eqs. (24) through (28) into a set of linear algebraic equations, (74)–(78).

The solution of Eqs. (74) through (78) is shown as follows:

$$U = \frac{-i[k_1(s + \alpha + ik_1u_0) + fk_2]}{(s + \alpha + ik_1u_0)^2 + f^2}\Phi \quad (81)$$

$$V = \frac{-i[k_2(s + \alpha + ik_1u_0) - fk_1]}{(s + \alpha + ik_1u_0)^2 + f^2}\Phi \quad (82)$$

$$W = \left\{\frac{-\tilde{I}(s)}{[(s + \alpha + ik_1u_0)^2 + f^2]}\frac{k^2}{(p + 1/h)(p^2 - k^2T^2)}\right\}dZ_Q + \frac{1}{p^2 - k^2T^2}\left\{p\tilde{W}(0, s) - \frac{(s + \alpha + ik_1u_0)k^2}{(s + \alpha + ik_1u_0)^2 + f^2}\tilde{\Phi}(0, s)\right\} \quad (83)$$

$$B = \left\{\frac{\tilde{I}(s)}{(s + \alpha + ik_1u_0)}\frac{1}{(p + 1/h)}\left[1 + \frac{k^2\dfrac{N^2}{(s + \alpha + ik_1u_0)^2 + f^2}}{p^2 - k^2T^2}\right]\right\}dZ_Q + \frac{1}{p^2 - k^2T^2}\left\{\frac{k^2N^2}{(s + \alpha + ik_1u_0)^2 + f^2}\tilde{\Phi}(0, s) - \frac{N^2}{s + \alpha + ik_1u_0}p\tilde{W}(0, s)\right\} \quad (84)$$

$$\Phi = \left\{\frac{\tilde{I}(s)}{(s + \alpha + ik_1u_0)}\frac{p}{(p + 1/h)(p^2 - k^2T^2)}\right\}dZ_Q + \frac{1}{p^2 - k^2T^2}\left\{p\tilde{\Phi}(0, s) - \frac{(s + \alpha + ik_1u_0)^2 + N^2}{s + \alpha + ik_1u_0}\tilde{W}(0, s)\right\}, \quad (85)$$

where

$$T = T(s) = \left[\frac{(s + \alpha + ik_1u_0)^2 + N^2}{(s + \alpha + ik_1u_0)^2 + f^2}\right]^{1/2}. \quad (86)$$

Next we use the inverse Laplace transform twice, $\mathcal{L}_{p,z}^{-1}$ and $\mathcal{L}_{s,t}^{-1}$, on (81)–(85) to solve for $dZ$s

$$dZ_u(k_1, k_2; z, t) = \mathcal{L}_{s,t}^{-1}\{\mathcal{L}_{p,z}^{-1}\{U\}\}$$

$$dZ_v(k_1, k_2; z, t) = \mathcal{L}_{s,t}^{-1}\{\mathcal{L}_{p,z}^{-1}\{V\}\}$$

$$dZ_w(k_1, k_2; z, t) = \mathcal{L}_{s,t}^{-1}\{\mathcal{L}_{p,z}^{-1}\{W\}\}$$

$$dZ_b(k_1, k_2; z, t) = \mathcal{L}_{s,t}^{-1}\{\mathcal{L}_{p,z}^{-1}\{B\}\}$$

$$dZ_\phi(k_1, k_2; z, t) = \mathcal{L}_{s,t}^{-1}\{\mathcal{L}_{p,z}^{-1}\{\Phi\}\}.$$

The inverse Laplace transform $\mathcal{L}_{p,z}^{-1}$ on Eq. (81) through (85) leads to

$$\tilde{U} = \mathcal{L}_{p,z}^{-1}\{U\} = \frac{-i[k_1(s + \alpha + ik_1u_0) + fk_2]}{(s + \alpha + ik_1u_0)^2 + f^2}\tilde{\Phi} \quad (87)$$

$$\tilde{V} = \mathcal{L}_{p,z}^{-1}\{V\} = \frac{-i[k_2(s + \alpha + ik_1u_0) - fk_1]}{(s + \alpha + ik_1u_0)^2 + f^2}\tilde{\Phi} \quad (88)$$

$$\tilde{W} = \mathcal{L}_{p,z}^{-1}\{W\} = \frac{-k^2h^2}{(1 - k^2h^2)}\frac{\tilde{I}(s)}{[(s + \alpha + ik_1u_0)^2 + \Lambda^2]}\left\{\exp\left(-\frac{z}{h}\right) - \cosh(zkT) + \frac{1}{hkT}\sinh(zkT)\right\}dZ_Q + \cosh(kzT)\tilde{W}(0, s) - \frac{s + \alpha + ik_1u_0}{(s + \alpha + ik_1u_0)^2 + f^2}\frac{k}{T}\sinh(kzT)\tilde{\Phi}(0, s) \quad (89)$$

$$\tilde{B} = \mathcal{L}_{p,z}^{-1}\{B\} = \frac{\tilde{I}(s)}{(s+\alpha+ik_1u_0)}\left\{\exp\left(-\frac{z}{h}\right) + \frac{k^2h^2}{1-k^2h^2}\frac{N^2}{[(s+\alpha+ik_1u_0)^2+\Lambda^2]}\left[\exp\left(-\frac{z}{h}\right) - \cosh(zkT) + \frac{1}{hkT}\sinh(zkT)\right]\right\}dZ_Q + \frac{k^2N^2}{(s+\alpha+ik_1u_0)^2+f^2}\frac{1}{kT}\sinh(kzT)\tilde{\Phi}(0,s) - \frac{N^2}{s+\alpha+ik_1u_0}\cosh(kzT)\tilde{W}(0,s) \quad (90)$$

$$\tilde{\Phi} = \mathcal{L}_{p,z}^{-1}\{\Phi\} = \frac{-h}{(1-k^2h^2)}\frac{\tilde{I}(s)}{(s+\alpha+ik_1u_0)}\frac{(s+\alpha+ik_1u_0)^2+f^2}{(s+\alpha+ik_1u_0)^2+\Lambda^2}\left\{\exp\left(-\frac{z}{h}\right) - \cosh(zkT) + hkT\sinh(zkT)\right\}dZ_Q + \cosh(kzT)\tilde{\Phi}(0,s) - \frac{(s+\alpha+ik_1u_0)^2+N^2}{s+\alpha+ik_1u_0}\frac{1}{kT}\sinh(kzT)\tilde{W}(0,s), \quad (91)$$

where

$$\Lambda^2 = \frac{f^2-k^2h^2N^2}{1-k^2h^2}. \quad (92)$$

The boundary conditions (79) and (80) require

$$\tilde{W}(0,s) = 0 \quad (93)$$

$$\tilde{\Phi}(0,s) = \frac{h}{(1-k^2h^2)}\frac{\tilde{I}(s)}{(s+\alpha+ik_1u_0)} \times \frac{(s+\alpha+ik_1u_0)^2+f^2}{(s+\alpha+ik_1u_0)^2+\Lambda^2}(khT-1)dZ_Q. \quad (94)$$

Thus, the solution of Eqs. (87) through (91) subject to the boundary conditions (93) and (94) is

$$\tilde{U} = \frac{-i[k_1(s+\alpha+ik_1u_0)+fk_2]}{(s+\alpha+ik_1u_0)^2+f^2}\tilde{\Phi} \quad (95)$$

$$\tilde{V} = \frac{-i[k_2(s+\alpha+ik_1u_0)-fk_1]}{(s+\alpha+ik_1u_0)^2+f^2}\tilde{\Phi} \quad (96)$$

$$\tilde{W} = \frac{-k^2h^2}{(1-k^2h^2)}\frac{\tilde{I}(s)}{[(s+\alpha+ik_1u_0)^2+\Lambda^2]} \times \left\{\exp\left(-\frac{z}{h}\right) - \exp(-zkT)\right\}dZ_Q \quad (97)$$

$$\tilde{B} = \frac{\tilde{I}(s)}{(s+\alpha+ik_1u_0)}\left\{\exp\left(-\frac{z}{h}\right) + \frac{k^2h^2}{1-k^2h^2}\frac{N^2}{[(s+\alpha+ik_1u_0)^2+\Lambda^2]} \times \left[\exp\left(-\frac{z}{h}\right) - \exp(-zkT)\right]\right\}dZ_Q \quad (98)$$

$$\tilde{\Phi} = \frac{-h}{(1-k^2h^2)}\frac{\tilde{I}(s)}{(s+\alpha+ik_1u_0)} \times \frac{(s+\alpha+ik_1u_0)^2+f^2}{(s+\alpha+ik_1u_0)^2+\Lambda^2}\left\{\exp\left(-\frac{z}{h}\right) - khT\exp(-zkT)\right\}dZ_Q. \quad (99)$$

Using the inverse Laplace transform $\mathcal{L}_{s,t}^{-1}$ on (95)–(99) results in the functional forms of $dZ$'s shown in section 3c.

## APPENDIX C

### Derivation of Eq. (53)

We may rewrite Eq. (51) using Eq. (5) as

$$\frac{\partial q}{\partial t} + u\frac{\partial q}{\partial x} + v\frac{\partial q}{\partial y} + w\frac{\partial q}{\partial z} = 0. \quad (100)$$

Linearly superimposing the synoptic wind $u_0$ on the thermally induced mesoscale flow component $u$, and substituting Eqs. (11)–(13) and (52) into Eq. (100), we have

$$\frac{\partial \overline{q}}{\partial t} + \frac{\partial q'}{\partial t} + u_0\frac{\partial q'}{\partial x} + u'\frac{\partial q'}{\partial x} + v'\frac{\partial q'}{\partial y} + w'\frac{\partial \overline{q}}{\partial z} + w'\frac{\partial q'}{\partial z} = 0, \quad (101)$$

where we have used the conditions $\overline{u} = 0$, $\overline{v} = 0$, and $\overline{w} = 0$.

Assuming the domain-averaged moisture profile $\overline{q}$ to be independent of time, implying $\overline{q} = \overline{q}(z)$, and dropping the cross products of the perturbation terms in Eq. (101) leads to the linearized equation for $q'$:

$$\frac{\partial q'}{\partial t} + u_0 \frac{\partial q'}{\partial x} + w' \frac{\partial \bar{q}}{\partial z} = 0. \qquad (102)$$

## REFERENCES


André, J. C., P. Bougeault, and J. P. Goutorbe, 1990: Regional estimates of heat and evaporation fluxes over nonhomogeneous terrain: Examples from the HAPEX-MOBILHY Programme. *Bound.-Layer Meteor.*, **50,** 77–108.

Avissar, R., and R. A. Pielke, 1989: A parameterization of heterogeneous land surfaces for atmospheric numerical models and its impact on regional meteorology. *Mon. Wea. Rev.*, **117,** 2113–2136.

——, and F. Chen, 1993: Development and analysis of prognostic equations for mesoscale kinetic energy and mesoscale (subgrid-scale) fluxes for large scale atmospheric models. *J. Atmos. Sci.*, **50,** 3751–3774.

Dalu, G. A., and R. A. Pielke, 1989: An analytical study of the sea breeze. *J. Atmos. Sci.*, **46,** 1815–1825.

——, and ——, 1993: Vertical heat fluxes generated by mesoscale atmospheric flow induced by thermal inhomogeneities in the PBL. *J. Atmos. Sci.*, **50,** 919–926.

——, ——, R. Avissar, M. Baldi, and A. Guerrini, 1991: Linear impact of thermal inhomogeneities on mesoscale atmospheric flow with zero synoptic wind. *Ann. Geophys.*, **9,** 641–647.

Hsu, H. M., 1987: Study of linear atmospheric flow above a finite surface heating. *J. Atmos. Sci.*, **44,** 186–199.

Lynn, B. H., F. Abramopoulos, and R. Avissar, 1995a: Using similarity theory to parameterize mesoscale heat fluxes generated by subgrid-scale landscape discontinuities in GCMs. *J. Climate,* **8,** 932–951.

——, D. Rind, and R. Avissar, 1995b: The importance of mesoscale circulations generated by subgrid-scale landscape heterogeneities in general circulation models. *J. Climate,* **8,** 191–205.

Pielke, R. A., G. A. Dalu, J. S. Snook, T. J. Lee, and T. G. F. Kittel, 1991: Nonlinear influence of mesoscale land use on weather and climate. *J. Climate,* **4,** 1053–1069.

Rabin, R. M., S. Stadler, P. Wetzel, D. J. Stensrud, and M. Gregory, 1990: Observed effects of landscape variability on convective clouds. *Bull. Amer. Meteor. Soc.*, **71,** 272–280.

Rotunno, R., 1983: On the linear theory of the land sea breeze. *J. Atmos. Sci.*, **40,** 1999–2009.

Segal, M., R. Avissar, M. C. McCumber, and R. A. Pielke, 1988: Evaluation of vegetation effects on the generation and modification of mesoscale circulations. *J. Atmos. Sci.*, **45,** 2268–2286.

Smith, E. A., and Coauthors, 1992: Area-averaged surface fluxes and their time–space variability over the FIFE experimental domain. *J. Geophys. Res.*, **97,** 18 599–18 622.

Stull, R. B., 1988: *An Introduction to Boundary Layer Meteorology.* Kluwer Academic, 666 pp.

Sun, J., and L. Mahrt, 1994: Spatial distribution of surface fluxes estimated from remotely sensed variables. *J. Appl. Meteor.*, **33,** 1341–1353.

Yaglom, A. M., 1987: *Correlation Theory of Stationary and Related Random Functions I.* Springer-Verlag, 512 pp.